Applied Catalysis B: Environmental 121–122 (2012) 190–197

Contents lists available at SciVerse ScienceDirect

Applied Catalysis B: Environmental

journal homepage: www.elsevier.com/locate/apcatb

# Nanocrystalline $TiO_2$ based films onto fibers for photocatalytic degradation of organic dye in aqueous solution

A. Panniello[b], M.L. Curri[b], D. Diso[d], A. Licciulli[d], V. Locaputo[a], A. Agostiano[b,c], R. Comparelli[b,*], G. Mascolo[a,**]

[a] CNR-IRSA Istituto di Ricerca sulle Acque, Bari Division, Via De Blasio 5, I-70132 Bari, Italy
[b] CNR-IPCF Istituto per i Processi Chimici e Fisici – Bari Division, c/o Dip. Chimica, Via Orabona 4, I-70126 Bari, Italy
[c] Università di Bari – Dip. Chimica, Via Orabona 4, I-70126 Bari, Italy
[d] Dipartimento Ingegneria dell'Innovazione, Università di Lecce, Via Monteroni, 73100 Lecce, Italy

ARTICLE INFO

*Article history:*
Received 27 December 2011
Received in revised form 10 March 2012
Accepted 20 March 2012
Available online 28 March 2012

*Keywords:*
$TiO_2$ colloidal nanocrystals
$TiO_2$ Degussa P25
Supported nano-sized $TiO_2$
Degradation of organic dye

ABSTRACT

Nanocrystalline titania ($TiO_2$) synthesized via sol–gel, by using an alkoxide precursor were deposited onto commercially available silica and alumina fibers, namely E-Glass and Nextel 650, respectively. Different processing conditions and material preparation parameters, such as amount of $TiO_2$, film composition and annealing temperature were tested in order to obtain nanocrystalline $TiO_2$ with different morphological and structural characteristics. The materials were characterized by scanning electron microscopy (SEM), X-ray diffraction (XRD), and the Brunauer, Emmett, and Teller (BET) surface area measurements. The photocatalytic activity of the obtained coated fibers was investigated by monitoring the degradation of a model molecule, an azo dye (Methyl Red), under UV irradiation in aqueous solution. The detected photocatalytic performance of the sol–gel derived nanocrystalline $TiO_2$ was explained on the basis of mechanism associated to the photocatalytic decomposition of organic molecules using semiconductor oxides and accounted for the structural and morphological characteristics of the $TiO_2$ based coating. The materials with the most suited characteristics for photocatalysis were used to scale up the deposition onto a larger sample of fiber and then tested in a photocatalytic reactor. A commercially available $TiO_2$ standard material ($TiO_2$ P25 Degussa) was used as reference, in order to ultimately assess the viability of the coating process for real application.



## 1. Introduction

In recent years, among the advanced oxidation processes (AOPs), the semiconductor-assisted photocatalytic methods have received great attention. Such a large interest derives from their relevant advantages that offers in terms of high efficiency for organic pollutants degradation and low cost of the employed catalyst [1]. In this perspective, $TiO_2$ represents the most widely used photocatalyst due to its chemical stability, commercial availability and excellent catalytic properties [2–5]. Nevertheless, the use of $TiO_2$ powders dispersed into aqueous media as a photocatalyst presents relevant technological drawbacks related to the catalyst recovery and recycle, which indeed are crucial for viable applications in water treatments in a large scale.

In order to overcome such technological limitations, many attempts have been made to immobilize catalysts onto substrates, such as glass beads, glass fibers, silica, stainless steel, textiles, honeycombs, activated carbon, and zeolites [6–14]. Design and implementation of novel $TiO_2$-based catalysts deposited onto suitable substrates is a challenging task to obtain materials exploitable for environmental applications. In addition a critical drawback of catalyst immobilization stays in the dramatic reduction of the active surface area, which consequently turns into a decrease of catalytic efficiency.

Nanosized $TiO_2$ is expected to reduce such loss of performance thanks to its extremely high surface-to-volume ratio which can greatly increase the density of active sites available for adsorption and catalysis. Moreover, the size-dependent band gap allows to tune the electron-hole red-ox potentials and thus to control selectivity in photochemical reactions. Also, the reduced dimensions of the nanocatalysts allow the photo-generated charges to readily migrate on the catalyst surface thus reducing the probability of undesired bulk recombination [15]. Anatase $TiO_2$, both in bulk and nanostructured form, is well known as one of the most efficient, non-toxic, and inexpensive photocatalyst [6]. Immobilization

* Corresponding author. Tel.: +39 080 5442027; fax: +39 080 5442128.
** Corresponding author. Tel.: +39 080 5820519; fax: +39 080 5313365.
*E-mail addresses:* r.comparelli@ba.ipcf.cnr.it (R. Comparelli), giuseppe.mascolo@ba.irsa.cnr.it (G. Mascolo).

0926-3373/$ – see front matter © 2012 Elsevier B.V. All rights reserved.
doi:10.1016/j.apcatb.2012.03.019

of nanostructured catalysts is needed to overcome technological issues related to nanocatalyst recovery and re-use. In principle the high surface to volume ratio is reasonable to compensate for the loss in performance deriving from deposition of nanoparticles onto a surface [6,7]. However we have recently demonstrated that in spite of the very high surface area the overall photocatalytic efficiency has not been demonstrated to overcome the performance of conventional catalyst in suspended form [16].

A possible solution, able to trade off such a crucial issue is the use of fibers. Fiber coating may represent a practical approach able to increase the surface area available for the aqueous phase being treated. $TiO_2$ coatings with submicron thickness have been prepared by different deposition techniques, such as sputtering, spray pyrolysis [17] and sol–gel processing [18]. In this perspective, the sol–gel method has been demonstrated to be an effective approach for the preparation of mechanically stable $TiO_2$ films deposited onto various substrates [19]. Such a chemical route usually requires thermal treatment at high annealing temperature in order to obtain the desired crystalline phase and, at the same time, a good adherence to a support [20] which can be conveniently selected, in terms of composition and geometry to maximize the amount of active sites accessible for photocatalysis. In addition, the photodegradation efficiency is renown to be related to the crystalline phase of the catalyst, being anatase regarded as more efficient than other phases, and to the grain dimensions [21], considering also that the specific surface area decreases as grain size increases.

In the present work, $TiO_2$ nanoparticles were synthesized in anatase phase by using a sol–gel route, namely a typical polymeric route was followed to produce $TiO_2$ nanoparticles from metal alkoxides, allowing the deposition of the nanostructured material, by dip-coating technique, onto non conventional supporting material, namely two types of commercially available fibers made of silica (E-Glass) and alumina (Nextel-720), respectively.

Several preparation parameters, such as $TiO_2$ nanocrystal (NC) amount, annealing temperature and deposition of a $SiO_2$ buffer, for preventing Na from the glass substrate to diffuse in the $TiO_2$ nanostructures, were tested. The morphological and structural characteristics of the obtained coatings were investigated by scanning electron microscope (SEM), X-ray diffraction (XRD) analysis, and the Brunauer, Emmett and Teller (BET) surface area measurements. The photocatalytic activity of the immobilized nanosized catalysts was then evaluated by a series of photodegradation experiments, carried out using Methyl Red (MR) as a model compound in order to (i) investigate the degradation mechanism, (ii) monitor the candidate materials with the highest photocatalytic performance for scale up experiments. For such a purpose $TiO_2$ Degussa P25 in an aqueous suspension was considered a reference.

## 2. Experimental

### 2.1. Materials and chemicals

Tetraisopropylorthotitanate $Ti(OCH(CH_3)_2)_4$ (TPOT) (purity ≥ 97%), tetraethylorthosilicate $Si(OC_2H_5)_4$ (TEOS) (purity ≥ 99%), 2-propanol and Methyl Red (MR) (2-(4-dimethylamino-phenylazo)-benzoic acid (C.I. 13020) were purchased from Sigma–Aldrich. Commercial $TiO_2$ was $TiO_2$ "Degussa P25" (nonporous anatase; surface area, 50 $m^2/g$; mean diameter, approximately 30 nm). All solvents were LC/MS grade and purchased from Aldrich. Water used for liquid chromatography as well as for preparing all aqueous solutions (18.2 MΩ cm, organic carbon content ≤ 4 μg/L) was obtained from a Milli-Q Gradient A-10 system (Millipore).

The silica fiber applied in this research is E-Glass, a low alkali glass product with a density of 2.55 $g/cm^3$ and with a typical nominal composition of $SiO_2$ 54% (w/w), $Al_2O_3$ 14% (w/w), CaO + MgO 22% (w/w), $B_2O_3$ 10% (w/w) and $Na_2O + K_2O$ less than 2% (w/w).

Nextel-720 alumina based fiber, manufactured by 3 M Corporation, has been used in this work. Such a fiber is an eight-harness satin fabric, with the tows in the fabric contain approximately 400 filaments, 10–12 μm in diameter, and 0/908 orientations, with a chemical composition approximately of 85% $Al_2O_3$ and 15% $SiO_2$ by weight.

### 2.2. Catalyst preparation and immobilization

Stable $TiO_2$ solutions were prepared by fast hydrolysis of TPOT in alcohol in the presence of high concentration of acid catalyst. TPOT was first dissolved in 2-propanol. Deionized water and HCl were diluted in 2-propanol and added to the Ti solution for hydrolysis. The components of the solution resulted in a [Ti]:[HCl]:[$H_2O$] = 1:1.35:6 molar proportion. Propanol content was calculated as the complementary weight in order to achieve 0.5%–2% (w/w) $TiO_2$ content in the sol assuming that all the Ti alkoxide moles are converted to $TiO_2$ after annealing. A fast hydrolysis followed by polycondensation and stabilization of nanosized amorphous $TiO_2$ particles takes place during the mixing. After 60 min a transparent colloidal solution is obtained. Silica sol (3% (w/w) $SiO_2$): TEOS and water were dissolved in the 2-propanol and mixed for 30 min under vigorous stirring and a temperature increase in the sol was observed, due the exothermic hydrolysis reaction. 1 N HCl was used as hydrolysis catalyzer previously diluted. The components of the solution resulted in a molar ratio [Si]:[HCl]:[$H_2O$] = 1:0.01:3.

Mean particle size as well as particle size distribution was measured by Dynamic Light Scattering (DLS), as reported below. The obtained particles resulted to have a particle size of 8 nm with a distribution of 4 nm (Fig. S1 in the Supporting material).

Two types of fibers were employed as supporting materials for the $TiO_2$ nanoparticles, namely an alumina- and a silica-based one. The alumina based material was Nextel fibers 720. These fibers have good mechanical properties, high thermal and chemical stability and a thermal expansion coefficient of $7.9 \times 10^{-6}$ m/°C. The Nextel fibers are thermally stable due to their homogeneous crystalline mix of α-alumina and mullite phases. The silica-based material was E-Glass fiber which was also selected to test as a cheaper alternative to alumina. Both fibers were used as substrates for $TiO_2$ based film deposition, after a thermal curing at 500 °C, which was carried out to remove the protective organic coating. Typically specific area of the alumina non porous fiber ranges from 0.11 to 0.15 $m^2/g$.

$TiO_2$ based coatings were applied by the dip coating from the sol, by using two different $TiO_2$ NC concentration, namely 0.5 and 2% (w/w). The used dip coating system works under controlled atmosphere, with independently adjustable dipping and withdrawal speeds. The withdrawal speed was selected in the range 1–10 cm/min and the humidity was kept below 50%. Different annealing temperatures were tested, from 300 to 400 °C. The temperature was then raised to the desired annealing temperature at heating rate of 10 °C/min and hold 60 min.

Each supported catalyst sample was prepared both with and without performing a pre-treatment step devoted to the deposition of a silica buffer layer, prior to the nanosized $TiO_2$ based film deposition. The buffer silica layer was steady on the fibers by means of a thermal treatment at 200 °C for 30 min. Overall, 16 different catalyst samples were prepared by following the conditions reported in Table 1 and subsequently tested for investigating their photocatalytic activity.

### 2.3. Photocatalytic experiments

Two different photoreactors were exploited. The whole set of fiber supported nanosized catalyst samples were tested by

**Table 1**
Characteristics of the different catalysts film immobilized onto silica and alumina fibers, respectively.

| Sample code | Fiber type | $TiO_2$ amount (%, w/w) | Silica layer | Annealing temperature (°C) |
|---|---|---|---|---|
| 1S | Silica | 0.5 | | 400 |
| 2S | Silica | 0.5 | X | 400 |
| 3S | Silica | 0.5 | | 300 |
| 4S | Silica | 0.5 | X | 300 |
| 5S | Silica | 2.0 | | 400 |
| 6S | Silica | 2.0 | X | 400 |
| 7S | Silica | 2.0 | | 300 |
| 8S | Silica | 2.0 | X | 300 |
| 1A | Alumina | 0.5 | | 400 |
| 2A | Alumina | 0.5 | X | 400 |
| 3A | Alumina | 0.5 | | 300 |
| 4A | Alumina | 0.5 | X | 300 |
| 5A | Alumina | 2.0 | | 400 |
| 6A | Alumina | 2.0 | X | 400 |
| 7A | Alumina | 2.0 | | 300 |
| 8A | Alumina | 2.0 | X | 300 |

using a quartz cuvette (1 cm × 1 cm × 4 cm) as a reactor. The fibers were suitably cut in order to fit the quartz cuvette geometry and positioned against the inner wall of the cuvette, perpendicularly to the light beam. Taking into account the fiber sample size (0.9 cm × 4.0 cm) and thickness (0.056 cm) and the different densities of Nextel-720 and E-Glass fiber (2.55 and 3.40 g/cm$^3$, respectively), 0.51 and 0.68 g of fiber (Nextel-720 and E-Glass, respectively) were used in each experiments. Experiments were performed at room temperature under air atmosphere. The photocatalytic experiments were performed by using MR water solutions with an initial dye concentration of 4 mg/L. A proper amount of either 0.1 N HCl or 0.1 N NaOH aqueous solutions, was added to the dye solution in order to achieve the desired pH, 2 or 6 respectively. The MR used for monitoring the photocatalytic activity of the supported catalysts, at pH 2 and 6, was kept under continuous mechanical stirring. The radiation source was a 250 W medium pressure mercury lamp ($\lambda > 250$ nm) with a fluence rate of 0.144 W/cm$^2$ (measured by a radiometer). Samples were withdrawn at scheduled times (up to 3 h) for residual MR concentration measurement. The coated fiber samples showing the highest photocatalytic activity in the above reported experimental conditions were selected for comparison with $TiO_2$ P25 Degussa powder in suspension in a scaled up reactor. For such purpose a 600 mL photoreactor was used, where a sheet (10 cm × 20 cm) of catalyst coated fiber was introduced and let it unfold along the wall of the photoreactor. Such a vessel was then filled with 500 mL of MR aqueous solution at concentration of 4 mg/L, and at pH 2 or 6, respectively. Due to the different geometry of the experimental set-up, a low pressure 17 W mercury lamp (Helios Italquartz, Italy), with a strong emission at 254 nm, was used as radiating source. The lamp was introduced into the glass reactor and kept fixed at the central axis of the reactor and separated from the aqueous solution by a quartz probe leading to a light path of 1.8 cm. All experiments were performed under ambient atmosphere, keeping the system under vigorous stirring. The low pressure UV lamp was characterized by uridine actinometry obtaining a fluence rate of 0.144 W/cm$^2$. A reference experiment employing $TiO_2$ P25 Degussa suspended in the photoreactor was carried out according to the optimized conditions reported in [16] in order to obtain a comparison of the supported nanosized catalysts performance with a standard catalyst. At scheduled irradiation times 5 mL of solution were withdrawn by means of a syringe. For the experiment carried out on the suspended catalyst, a centrifugation was necessary before the high performance liquid chromatography-mass spectrometry (HPLC/MS) analysis.

### 2.4. Analytical determinations

*Catalyst characterization.* The microstructure of $TiO_2$ was investigated by XRD at room temperature. Test samples were obtained by mechanically removing the coating from the fibers after drying. The crystallite size of $TiO_2$ was calculated by the Scherrer formula from the full width at half maximum of the main peak. The width of the peak was measured by Lorentzian fit of anatase peak at 25.28°. The morphology of the coating was investigated by scanning electron microscopy using a EVO-40 system (Zeiss). BET surface area (Kelvin 1042 equipment) and pore size distributions were measured on powders obtained peeling off the coating from the fibers.

Dynamic light scattering (DLS) was used to monitor the hydrodynamic diameter of $TiO_2$ nanoparticles employing a Malvern Zetasizer Nano S, model ZEN 1600 (Malvern Instruments, United Kingdom). The DLS was operated with a He–Ne laser at a wavelength of 633 nm and light scattering was detected at an angle of 173°. Measurements were carried out using freshly prepared samples that were filtered using 0.2 μm Anotop 10 inorganic membrane filter (Whatman) to remove any interfering dust particles. DLS measurements were performed at 25 °C.

*Elemental analysis.* The determination of dissolved Ti concentration was performed by inductively coupled plasma optical emission spectroscopy (ICP-OES) analysis using an Optima 3000 instrumentation (Perkin-Elmer). Total amount of $TiO_2$ deposited onto fibers was determined by mineralizing a small piece of the fibers (about 1 g) and then determining the Ti concentration of the obtained acidic solutions using ICP-OES. The release of catalyst into water solution was evaluated by mineralizing 20 mL of the aqueous phase and then the Ti concentration was determined by ICP-OES.

*MR decay and by-products formation.* MR photocatalytic decolouration was monitored by using a UV–vis Cary 5000 spectrophotometer (Varian). In addition, HPLC/MS–MS analysis was used to determine residual dye concentration and by-product identification by using an Acquity chromatographic system, equipped with both an auto-sampler and a photo-diode array detector (Waters), interfaced to an API 5000 mass spectrometer (AB Sciex) by means of a turboionspray interface. 5 μL samples were injected by a Rheodyne valve and a 10 μL loop, and eluted at 0.3 mL/min through a HSS T3 C18 column, 2.1 mm × 150 mm, 1.8 μm, with the following gradient: from 95/5 A/B (A: water/MeOH 95/5 + ammonium acetate 1.5 mM; B: MeOH + ammonium acetate 1.5 mM) to 0/100 in 12 min, which has been then maintained for 3 min. The MS interface conditions were as follows: needle voltage, 4000 V; declustering potential, 120 V; mass range, 50–500 Th; scan time, 0.3 s; nebulizer gas flow (air), 1.5 L/min; curtain gas flow (nitrogen), 1 L/min; auxiliary gas flow (air) delivered by a turbo-V heated probe, 6 L/min at 450 °C. Injections were performed in duplicate and residual dye concentration values were obtained by using a proper calibration curve.

Dissolved organic carbon (DOC) was measured on filtered samples (0.45 μm) by a Shimadzu TOC-VCSH analyzer.

## 3. Results and discussion

### 3.1. Microstructural and morphological characterization of the supported catalysts

In order to perform the microstructural characterization of the supported nanosized $TiO_2$, the catalysts were prepared as powders. The XRD investigation carried at room temperature on samples treated with increasing temperature demonstrated that anatase formation occurs at 250 °C whereas the rutile formation can be achieved starting from 600 °C (data not reported). In Fig. 1, the sample diffractograms are reported at 300 °C and 400 °C. The crystallite

**Table 2**
Main characteristics of the nano-$TiO_2$ catalysts prepared as powders.

| Annealing temperature (°C) | $TiO_2$ NC grain size[a] (nm) | BET surface area ($m^2/g$) |
|---|---|---|
| 300 | 3.2 ± 0.6 | 82.5 |
| 400 | 8.3 ± 1.6 | 72.5 |

[a] Estimated by XRD applying the Debye–Scherrer formula.

size of $TiO_2$ was calculated from XRD diffractograms by the application of the Scherrer formula, by Lorentzian fit of anatase peak at 25.28°. As expected, the crystal size is observed to increase with the increase of the thermal treatment temperature. The grain crystal diameter of sample treated at 300 °C is 3.2 ± 0.6 nm, whereas the grain diameter of sample treated at 400 °C is 8.3 ± 1.6 nm. BET analysis performed on $TiO_2$ powders treated at 400 °C is reported in Table 2. The obtained results are in a good agreement with the data obtained from the XRD analyses, since the surface area decreases, and concomitantly the grain size increases, as the treatment temperature increases.

The morphological analysis of nanosized $TiO_2$ coated silica and alumina fibers was performed by SEM in order to investigate the coating features, namely adhesion, and morphology. In Fig. 2, panel 1, SEM images of two coated silica fibers at different $TiO_2$ content are compared (Samples 4S and 8S, respectively), highlighting that the coating obtained from a more concentrated solution exhibits a texture with interconnected cracks and results detached in some regions. Despite the occurrence of such detachment of the coatings, elemental ICP-OES spectroscopic analyses have revealed that Ti ion content in the aqueous solution is below the detection limit of the technique (<0.01 mg/L). It could be tentatively proposed that such cracks cause a $TiO_2$ film detachment by simply handling the fiber, prior to its immersion in MR water solution.

The cracks in the coatings significantly reduce the adhesion of the coatings and their mechanical quality. The cracks exhibited by the coating derived from concentrated sols can be explained assuming that the critical thickness is exceeded. It has been established that during the drying stage a pressure gradient develops in the liquid phase of the gel resulting in differential shrinkage of the sol–gel network [22]. The film surface shrinks faster than its inner layer, and this induces the appearance of a tensile stress in the film surface. The maximum tensile stress occurs at the drying surface of the film, and according to the model of Brinker [23], depends on viscosity, permeability of the network, the rate of evaporation and the viscosity of the liquid, and film thickness. Fracture of the film occurs when the tensile stress exceeds the strength of the gelled network [24].

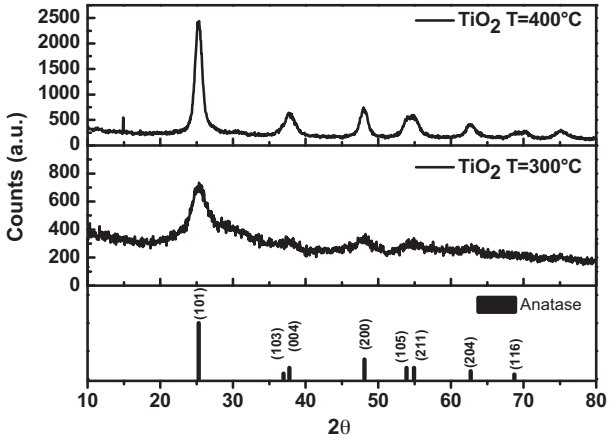


**Fig. 1.** XRD diffractograms of titania powders after annealing at 300 °C and 400 °C. In the column diagram the standard $TiO_2$ anatase diffraction peak are reported.

Higher photocatalytic efficiency was achieved with supported catalyst with higher $TiO_2$ loading, in agreement with similar data reported in literature (see next paragraph). Such a result could be reasonably accounted for the $TiO_2$ content in the deposited coating on the fiber, irrespectively of the morphology. In fact the thickness, and, consequently, compactness and adhesion, of the film could be affected by the loading of the deposited $TiO_2$ layer, ultimately resulting in a detachment of the film. Similar features were found for the coatings deposited onto alumina fibers treated at 300 °C (Fig. 2, panel 2) thus confirming, also for this material, a morphology which is indicative of poor adhesion and low compactness of the coating.

Conversely, improved adhesion and compactness of the coating were observed by treating at 400 °C, the 2% (w/w) $TiO_2$ coated alumina support without any buffer (Fig. 2, panel 3). In particular, the morphology investigation shows a very good adhesion and stability of the coating which shows only limited alteration after repeated handling and exposure to the aqueous solution under vigorous stirring (Fig. 2, panel 3b). This material showed the best photocatalytic efficiency (see below).

### 3.2. Photocatalytic activity investigation

The different sol–gel nanosized $TiO_2$ based catalysts deposited onto fibers were tested by monitoring the UV–vis absorbance spectra of a model compound (MR) and following the decay of the main dye absorption peak, namely 430 nm at pH 6 and 520 nm at pH 2 (Fig. S2). Such an approach is based on the assumption that the concentration of by-products absorbing at the same wavelength of the parent dye should be negligible with respect to MR concentration, in consideration of the good agreement between the results obtained by optical and chromatographic investigation of the reaction time course, as previously reported [4].

The efficiency of the prepared photocatalysts was compared by evaluating the percentage of the decolouration of MR after 3 h irradiation. Control experiments were also performed without supported catalyst in order to evaluate possible dye bleaching due to the UV irradiation only. In all cases only a negligible bleaching was observed. A comparison of the final catalytic efficiency for all the tested samples allowed to investigate the effect of processing and deposition conditions on the photocatalyst efficiency. For the set of nanosized $TiO_2$ coated silica fibers (E-Glass fiber, Samples 1S–8S, Table 1), generally, the presence of the silica buffer layer was found to decrease the photocatalytic activity of the investigated samples, irrespectively of annealing temperature and $TiO_2$ concentration of the starting sol (Fig. 3, panels A and B).

In particular, in the case of lower annealing temperature, a more pronounced deactivation was found for lower $TiO_2$ content catalyst in presence of a buffer layer (4S) with respect to the unbuffered counterpart (3S). When treated at 400 °C, the buffered sample at higher $TiO_2$ content (6S) showed a lower photocatalytic efficiency with respect to its unbuffered equivalent (5S). For one sample (2S), prepared at 400 °C with 0.5% (w/w) $TiO_2$, a slightly higher efficiency was found in presence of the silica buffer layer. Samples prepared at 2% (w/w) $TiO_2$ generally resulted in higher photocatalytic performance upon annealing at 400 °C, conversely lower annealing temperature turned in higher performance for lower $TiO_2$ concentration, despite higher annealing temperature cause a grain size

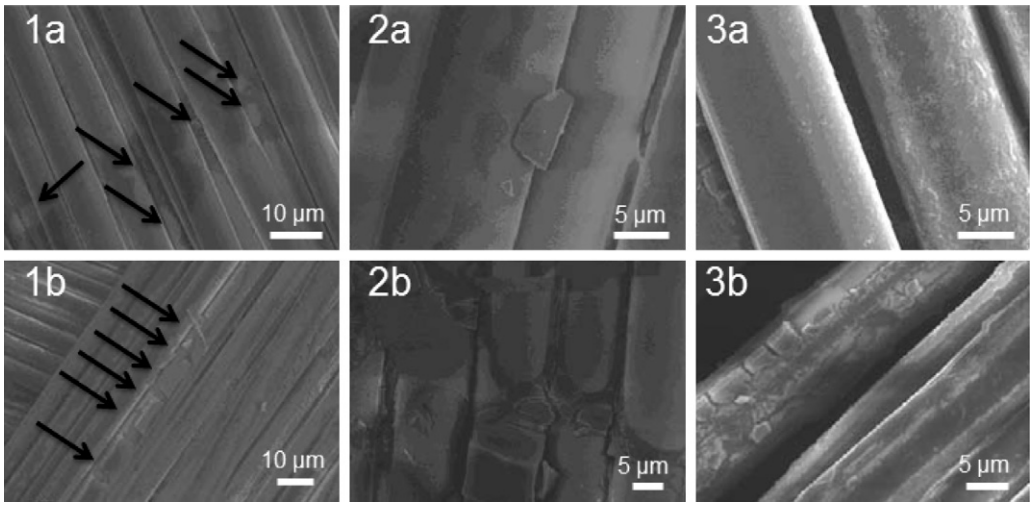


**Fig. 2.** SEM micrographs of: (i) silica fibers coated from solution at (1a) 0.5% (w/w) (Sample 4S) and (1b) 2.0% (w/w) (Sample 8S) $TiO_2$ content, both treated at 300 °C for 1 h; (ii) alumina coated fibers from solution at (2a) 0.5% (w/w) (Sample 3A) and (2b) 2.0% (w/w) (Sample 7A) $TiO_2$ content, both treated at 300 °C for 1h; (iii) alumina coated fiber from solution at 2.0% (w/w) $TiO_2$ content, treated at 400 °C for 1 h, before (3a) and after (3b) the photocatalytic experiment.

increasing and a lower surface area. Sample 3S (Fig. 3, panel B) was found to provide the highest performance in terms of catalytic efficiency, with 77% decolouration after the 3 h irradiation time.

As far as the investigated alumina fiber supported catalysts (Nextel-720, Samples 1A–8A, Table 1), the samples coated with silica buffer typically resulted in a lower photocatalytic activity, apart from Sample 2A, prepared at 400 °C with a 0.5% (w/w) $TiO_2$ concentration (Fig. 3, panel D). A very low efficiency was recorded for the 2% (w/w) $TiO_2$ loaded fibers (6A and 8A), irrespectively of the annealing temperature, while 0.5% (w/w) $TiO_2$ catalysts (2A, 4A) showed different efficiency according to the thermal treatment temperature (Fig. 3, panels C and D). At 400 °C the catalytic activity of the coated fibers was generally higher with respect to the result obtained by annealing 300 °C, despite the lower surface area (Table 2). Furthermore, an increase of $TiO_2$ content was found irrelevant to the photocatalytic activity in the case of 300 °C treated fibers, while the same $TiO_2$ concentration resulted in a higher efficiency for samples treated at 400 °C. In the whole set of alumina coated fibers, Sample 5A (i.e. 2% (w/w) $TiO_2$ and 400 °C annealing temperature) provided the complete dye decolouration during the entire irradiation time (Fig. 3, panel C).

In summary, the investigated preparative conditions resulted in photocatalytic performances varying within a rather narrow range, apart from some small fluctuations and generally below 50%. The presence of the buffer layer was generally found detrimental for photocatalytic activity of the coated fibers, and higher annealing temperature (400 °C) generally provide enhanced photoactivity. It could be tentatively proposed that the presence of buffer layer affects the stability of $TiO_2$ film, probably due to adhesion issues. Indeed, SEM micrographs in Fig. 2 (panel 1a and b) show several cracks. The effect of $TiO_2$ content should be considered in combination with the effect of annealing temperature. In fact, the SEM micrographs (panel 2a and 2b) show several cracks irrespectively of the $TiO_2$ content for fibres treated at 300 °C. On the other hand,

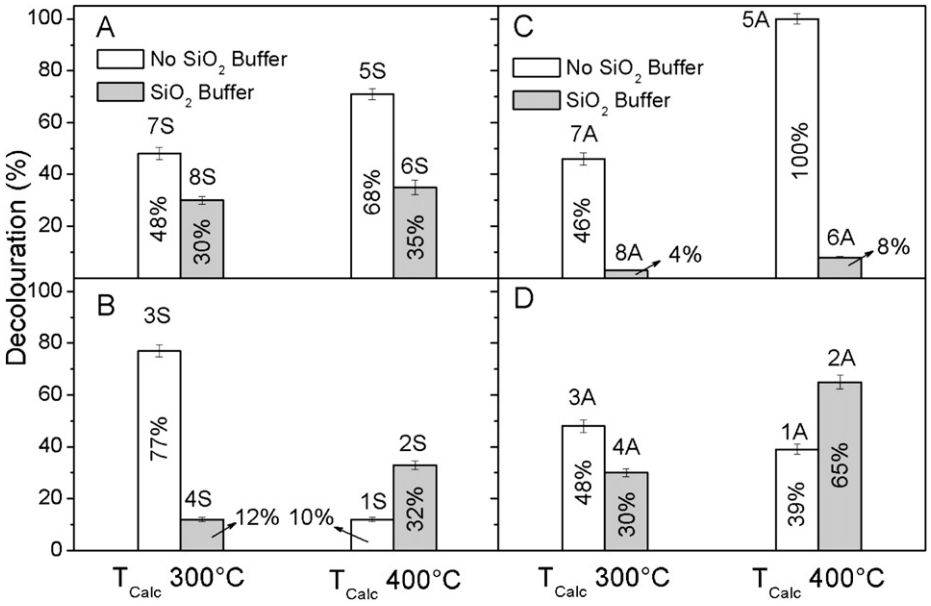


**Fig. 3.** MR decolouration catalyzed by: (i) silica fibers coated from solution at 2% (w/w) (A) and 0.5% (w/w) (B) of $TiO_2$ content; (ii) alumina fibers coated from solution at 2% (w/w) (C) and 0.5% (w/w) (D) of $TiO_2$ content, in the absence (white) and in the presence (light grey) of $SiO_2$ protective layer as a function of the annealing temperature. [MR]$t = 0 = 4$ mg/L. Data are reported as ±standard deviation obtained by three replicates.

an increase of annealing temperature for the same $TiO_2$ loading (400 °C, Sample 5A, SEM Picture 3a and b) leads to a compact and stable film, still clearly visible on the fiber after repeatedly handling. It could be thus proposed that the presence of several cracks could somehow reduce the amount of $TiO_2$ film prior its immersion in MR water solution, thus explaining the lower photoactivity. The residual film on the fiber could be stable enough to be resistant against mechanical stirring of the solution, thus accounting for the absence of Ti ion in water according to ICP-OES analyses.

In conclusion, Sample 3S, obtained without buffer layer, with 0.5% (w/w) $TiO_2$ at 300 °C and Sample 5A, prepared without buffer layer, with 2% (w/w) $TiO_2$ at 400 °C resulted the most efficient catalysts for the two series of investigated samples, silica and alumina fiber based, respectively. Therefore these types of samples were selected for the following scale up experiments.

### 3.3. Photocatalytic efficiency of $TiO_2$ coated fibers vs. suspended catalyst

The photocatalytic performance of the two selected types of coated silica and alumina fibers, respectively, was evaluated in scaled-up experiments, considering as a reference an aqueous suspension of $TiO_2$ Degussa P25. For this purpose a 600 mL reactor was employed, in order to allow an effective comparison of the performance of the fiber supported catalysts and Degussa P25 suspended sample, in a volume reasonable for pilot test.

Suspended catalyst was employed at 0.022 g/L since preliminary tests (performed in the concentration range 0.001–1 g/L) demonstrated that MR degradation rate maximized between 0.01 and 0.022 g/L (Fig. S3). This reflects the fact that the photocatalytic degradation is a balance of two opposite phenomena. The first is related to the active surface of the catalyst leading to higher degradation rate at higher catalyst concentration. The second is related to the light penetration which is higher at lower catalyst concentration. It follows that by increasing the catalyst concentration the degradation rate also increases but then reaches a plateau and then start to decrease because of the light scattering at high catalyst concentration. Decays of MR concentration during irradiation time are displayed in panel A of Fig. 4 for both supported and suspended catalysts. The results show that: (i) for all investigated catalysts MR is degraded faster at pH 2, (ii) the catalyst efficiency has the following trend: nano-$TiO_2$ on alumina fiber < nano-$TiO_2$ onto silica fiber < suspended Degussa P25 and (iii) all reactions follow an exponential decay, thus suggesting first-order kinetics. However, the log-plot of the MR concentration shows for all supported catalysts to follow two different first-order kinetics, with a faster decay at longer reaction time (Fig. 4, panel B). This behaviour can be consistent with a rate-limiting step occurring in the early stage of reaction, when the surface sites available for catalysis are all occupied by MR adsorbed molecules. Consequently during the early stage the MR degradation is controlled by the diffusion of new molecules that replace those just degraded to form by-products. At longer reaction times when the MR concentration has dropped a high extent of surface sites is available for the degradation reaction and, therefore, degradation rate increases. Interestingly, the same behaviour was observed at both pH 2 and 6. The measured first-order rate constants (Table 3) show that a speed-up effect of a factor of 2 occurs at longer reaction time for the two fibers and the investigated pH values.

The first-order rate constants reported in Table 3 also indicate that the performance of Degussa P25 catalyst is generally higher than that observed for the supported nano-$TiO_2$. However the degradation rate for the nano-$TiO_2$ onto alumina fiber, at longer reaction time, approaches that obtained with the Degussa P25 catalyst (0.081 $min^{-1}$ with respect to 0.105 $min^{-1}$). It follows that it would be possible to get some improvements in the performance

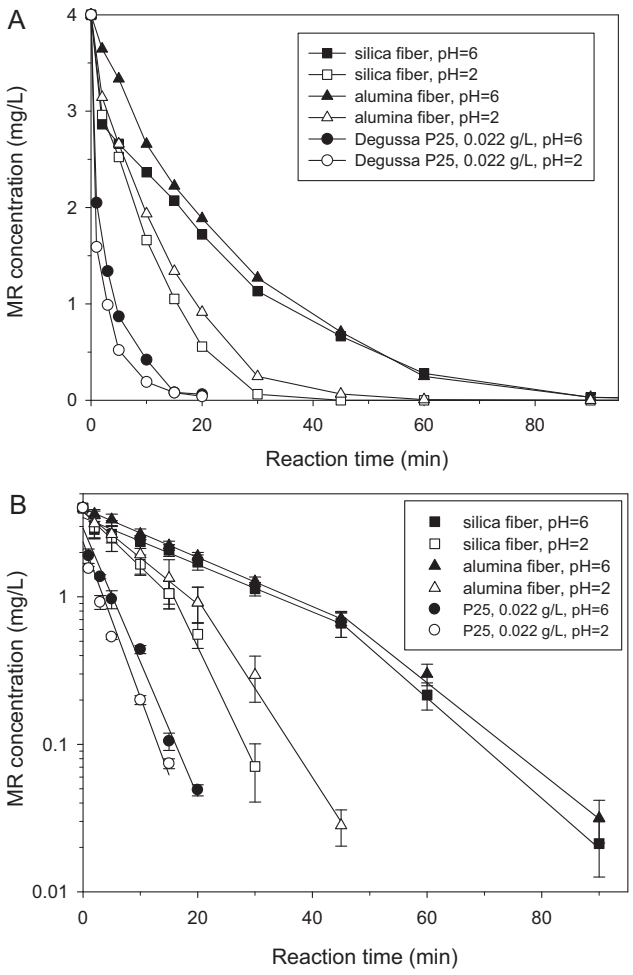


**Fig. 4.** (A) Comparison among the MR concentration decays during UV irradiation, at pH 2 and 6, in the presence of $TiO_2$ coated silica and alumina fibers, prepared in the same condition of Samples 3S and 5A, respectively, and $TiO_2$ Degussa P25 powder in suspended form. In panel (B) are reported the same decays for $TiO_2$ coated silica and alumina fibers on log C scale showing the two sections of pseudo-first order decays. The calculated first-order constants are reported in Table 3. Error bars represent standard deviation on 5 measurements.

of the supported fiber, by either enhancing the deposition method or employing more fiber in the reactor, in order to get a photocatalytic efficiency as high as, or even higher than that of Degussa P25 catalyst.

As far as the comparison of the absolute amount of employed catalysts is concerned, from Table 3 it is possible to note that the $TiO_2$ amount deposited onto the silica fiber (that with lesser efficiency) was two-fold that of alumina fiber which, in turn, was about eight times higher than that employed as a suspension. The much different absolute amount of catalyst deposited on the two fibers depends from the deposition method not perfectly optimized. Nevertheless, the obtained results suggest that probably the deposition procedure causes a multi-layer nanoparticle structure where the inner layers are not able to participate in the photocatalytic process.

Pseudo-first order kinetic constants (Table 3) also show that pH has a similar influence for both suspended and supported $TiO_2$ that MR degradation faster at acidic pH. However, for both alumina and silica fibers supported with nano-$TiO_2$ the effect was more pronounced. In fact, the increase of rate constants was 130% and 80% for nano-$TiO_2$ supported onto silica and alumina fiber, respectively. Such a rate increase was, within experimental error, identical at early as well as at longer stage of the reaction for both supported fibers. Instead, for Degussa P25 catalyst the rate constant increased

**Table 3**
First-order constants ($k$) of MR decomposition during photocatalytic reactions with immobilized $TiO_2$ nanoparticles and suspended $TiO_2$ Degussa P25.

| Employed catalyst | $k$ ($min^{-1}$) | | | | Absolute amount of catalyst (mg of $TiO_2$) |
|---|---|---|---|---|---|
| | pH = 2 | pH = 6 | | | |
| Degussa $TiO_2$ (suspended) | 0.105 ± 0.015 | 0.090 ± 0.011 | | | 11 |
| | Reaction time ($t_r$) range (min) | | Reaction time ($t_r$) range (min) | | |
| | $0 < t_r < 20$ | $t_r > 20$ | $0 < t_r < 45$ | $t_r > 45$ | |
| $TiO_2$ onto alumina fiber | 0.037 ± 0.005 ($R^2$ = 0.90) | 0.081 ± 0.010 ($R^2$ = 0.93) | 0.016 ± 0.001 ($R^2$ = 0.94) | 0.034 ± 0.005 ($R^2$ = 0.96) | 80 |
| $TiO_2$ onto silica fiber | 0.031 ± 0.005 ($R^2$ = 0.85) | 0.060 ± 0.006 ($R^2$ = 0.96) | 0.017 ± 0.002 ($R^2$ = 0.98) | 0.031 ± 0.003 ($R^2$ = 0.97) | 157 |

of just 17%. The obtained result can be explained taking into account that at acidic pH the presence of positive charge on titania surface can make the photogenerated electrons to reach more readily the catalyst surface. This, in turn, prevents detrimental electron-hole recombinations leading to higher reaction rate [6]. This effect is more evident when the surface area is higher. Therefore, as the BET surface area (Table 1) of supported catalysts is much higher than P25 this effect is much more evident for the former catalyst.

The mineralization extent during the photocatalytic degradation of MR was also evaluated by determining DOC at scheduled times. Obtained results (Fig. 5) are consistent with MR decays of Fig. 4, panel A since DOC removal was higher at pH 2 for both investigated supported nano-$TiO_2$ fibers. Nano-$TiO_2$ onto silica showed slightly higher DOC mineralization yield at pH 6, at longer reaction time. Instead, at pH 2 the removal percentages were practically the same for both supported catalysts. The finding that at longer reaction time, namely higher than 80 min, MR was completely removed but an high fraction of DOC was still present suggests that some degradation by-products should have been formed. Their investigation was performed by HPLC/MS–MS and compared to that carried out during MR degradation using the Degussa P25 catalyst in order to evaluate possible difference in degradation mechanism. It was found that the same by-products were detected for photocatalysis performed with both supported nano-$TiO_2$ fibers and Degussa P25. A similar result was previously obtained with nanoparticles of $TiO_2$ (prepared by a non-hydrolytic route) deposited onto the inner walls of a glass photoreactor [16]. The chemical structures of the detected by-products (Table S1) are consistent with two distinct degradation mechanisms, independently occurring. They are based on oxidation of methyl groups of MR by $O_2^{\bullet -}$ generated through $O_2$ reduction by free photoelectrons in the conduction band of the catalyst and on formation of hydroxyl radicals. In addition, the temporal evolution profiles of detected by-products (Fig. 6) show, as expected, a bell-shape with a maximum of formation between 10 and 30 min. This result confirms that the prepared fibers with supported nano-$TiO_2$ have a photocatalytic efficiency much higher than previously prepared nanoparticles of $TiO_2$ and deposited onto the inner walls of a glass photoreactor [16]. At longer reaction time no by-products were detected suggesting the formation of low molecular weight organic acids not amenable to HPLC/MS [25]. These compounds, that do not represent a toxicity issue, would account for the residual DOC present in the reaction mixture at long reaction time.

Finally, when working with $TiO_2$ deposited on substrates two important issues are worth to be carefully considered. They are related to (i) the stability of the supported catalyst and (ii) the release of catalyst to the aqueous solution. Repeated MR degradation was carried out showing that the efficiency of the supported catalyst remained unchanged over ten reaction (Fig. S4), despite repeated handling and washing of the fiber under running water. Such result demonstrates the stability of the $TiO_2$ film as already evidenced by SEM picture (Fig. 2, panel 3a and b). As for any possible release of the catalyst, at the end of each photocatalytic experiment a proper volume of aqueous solution was mineralized and analyzed for Ti by ICP-OES. Analytical results showed that Ti concentration was always below the detection limit of the technique (<0.010 mg/L).

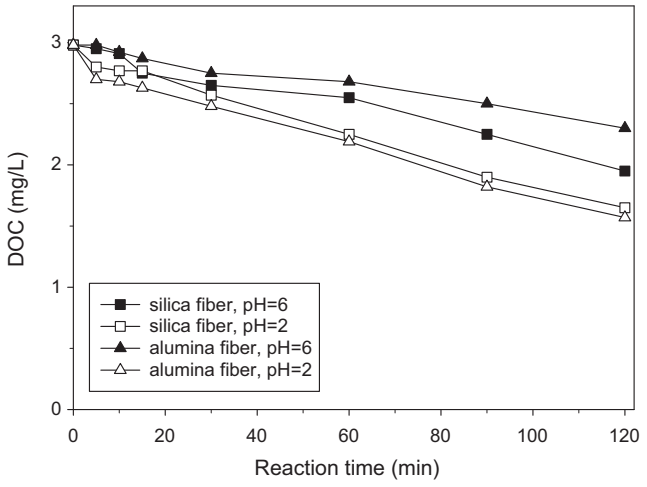


**Fig. 5.** DOC decay during UV irradiation of MR, at pH 2 and 6, in the presence of $TiO_2$ coated silica and alumina fibers, prepared in the same condition of Samples 3S and 5A, respectively.

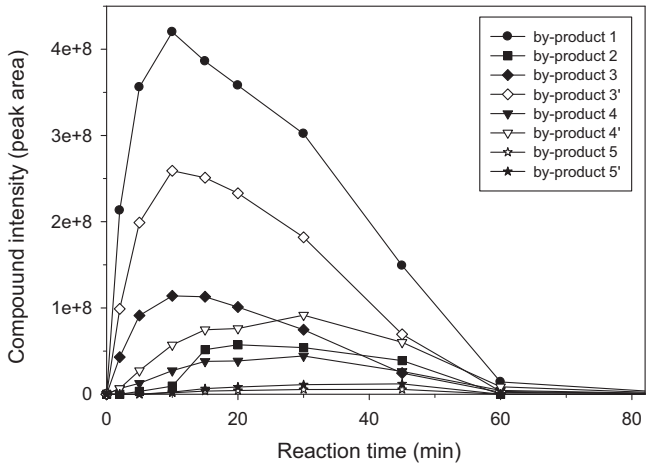


**Fig. 6.** Formation/degradation profiles of identified by-products during UV irradiation of MR at pH 6 in the presence of $TiO_2$ coated alumina fiber.

## 4. Conclusions

Alumina and glass fibers were effectively coated with anatase $TiO_2$ nanocrystalline film and the structure and morphological features of the final materials were investigated as a function of their photocatalytic performance in view of the use of such novel photocatalytic material for decomposition of environmental pollutants in aqueous matrix. First, the characteristic photocatalytic performances were screened in order to evaluate for the different prepared systems. For this purpose morphology and microstructure of the coating materials as well as the efficiency in the photocatalytic decolouration process were evaluated and the proper processing parameters were selectively chosen. In particular, it has been demonstrated that the presence of the silica buffer reduces the degradation performances of the catalysts both on alumina and glass fibers. In both cases the presence of the silica buffer has induced a detachment of the coating. A low compactness and bad adhesion to the substrate is generally exhibited by coatings treated at 300 °C, with a more extensive coating degradation observed at increasing coating thickness. Alumina fibers coated with a 2.0% (w/w) $TiO_2$ and thermally treated at 400 °C and without any buffer show remarkable results, thus demonstrating promising materials.

These features, combined with their high mechanical resistance to abrasion, make the material, prepared under these conditions, interesting and valuable candidates for filters for treating waste water (or even gases and vapors), being able to compensate for the loss of performances expected in the case of immobilized catalysts, and thus representing a truly innovative and promising result. In this perspective the photocatalytic degradation process of the most successful candidate has been performed in a reactor to test the performance on a larger scale and thus provide a more direct and reliable indication of the practical viability and its possible application in real systems.

## Acknowledgements

This work was partially supported by Apulia Region by funding Rela-Valbior project within the Scientific Research Framework Program 2007–2013, the explorative project PE_049 and the Strategic Project “Protection, consolidation and cleaning of stones characteristic of Apulia region: experimental analysis of environmental friendly products and monitoring of the treatments” (PS_083) within the Scientific Research Framework Program 2006.

## Appendix A. Supplementary data

Supplementary data associated with this article can be found, in the online version, at doi:10.1016/j.apcatb.2012.03.019.

## References

[1] S. Malato, P. Fernández-Ibáñez, M.I. Maldonado, J. Blanco, W. Gernjak, Catalysis Today 147 (2009) 1–59.
[2] X. Chen, S.S. Mao, Chemical Reviews 107 (2007) 2891–2959.
[3] W. Bahnemann, M. Muneer, M.M. Haque, Catalysis Today 124 (2007) 133–148.
[4] D. Nasuhoglu, V. Yargeau, D. Berk, Journal of Hazardous Materials 186 (2011) 67–75.
[5] L. Rizzo, S. Meric, M. Guida, D. Kassinos, V. Belgiorno, Water Research 43 (2009) 4070–4078.
[6] R. Comparelli, E. Fanizza, M.L. Curri, P.D. Cozzoli, G. Mascolo, R. Passino, A. Agostiano, Applied Catalysis B: Environmental 55 (2005) 81–91.
[7] M.K. Aminian, N. Taghavinia, A. Irajizad, S.M. Mahdavi, The Journal of Physical Chemistry C 111 (2007) 9794–9798.
[8] H.-W. Chen, Y. Ku, Y.-L. Kuo, Water Research 41 (2007) 2069–2078.
[9] A. Danion, J. Disdier, C. Guillard, N. Jaffrezic-Renault, Journal of Photochemistry and Photobiology A: Chemistry 190 (2007) 135–140.
[10] R. Kavitha, S. Meghani, V. Jayaram, Materials Science and Engineering B 139 (2007) 134–140.
[11] L. Rizzo, J. Koch, V. Belgiorno, M.A. Anderson, Desalination 211 (2007) 1–9.
[12] Y. Zhiyong, E. Mielczarski, J. Mielczarski, D. Laub, P. Buffat, U. Klehm, P. Albers, K. Lee, A. Kulik, L. Kiwi-Minsker, A. Renken, J. Kiwi, Water Research 41 (2007) 862–874.
[13] R. Comparelli, P.D. Cozzoli, M.L. Curri, A. Agostiano, G. Mascolo, G. Lovecchio, Water Science and Technology 49 (2004) 183–188.
[14] P.S.M. Dunlop, A. Galdi, T.A. McMurray, J.W.J. Hamilton, L. Rizzo, J.A. Byrne, Journal of Advanced Oxidation Technologies 13 (2010) 99–106.
[15] A.L. Linsebigler, G. Lu, J.T. Yates, Chemical Reviews 95 (1995) 735–758.
[16] G. Mascolo, R. Comparelli, M.L. Curri, G. Lovecchio, A. Lopez, A. Agostiano, Journal of Hazardous Materials 142 (2007) 130–137.
[17] H. Yanagi, Y. Ohoka, T. Hishiki, K. Ajito, A. Fujishima, Applied Surface Science 113–114 (1997) 426–431.
[18] T. Yoko, A. Yuasa, K. Kamiya, S. Sakka, Journal of The Electrochemical Society 138 (1991) 2279–2285.
[19] Y. Chen, E. Stathatos, D.D. Dionysiou, Surface and Coatings Technology 202 (2008) 1944–1950.
[20] A. Fernández, G. Lassaletta, V.M. Jiménez, A. Justo, A.R. González-Elipe, J.M. Herrmann, H. Tahiri, Y. Ait-Ichou, Applied Catalysis B: Environmental 7 (1995) 49–63.
[21] K.Y. Jung, S.B. Park, S.-K. Ihm, Applied Catalysis A: General 224 (2002) 229–237.
[22] G.W. Scherer, Journal of Non-Crystal Solids 109 (1989) 171–182.
[23] J.C. Brinker, G.W. Scherer, Sol–Gel Science: The Physics and Chemistry of Sol–Gel Processing, Academic Press, San Diego, CA, 1990.
[24] A. Díaz-Parralejo, A.L. Ortiz, R. Caruso, F. Guiberteau, Surface and Coatings Technology 205 (2011) 3540–3545.
[25] G. Mascolo, A. Lopez, A. Detomaso, G. Lovecchio, Journal of Chromatography A 1067 (2005) 191–196.